JEM Journal of Experimental Medicine

BRIEF DEFINITIVE REPORT

Microglial translational profiling reveals a convergent APOE pathway from aging, amyloid, and tau

Silvia S. Kang[1], Mark T.W. Ebbert[1], Kelsey E. Baker[1], Casey Cook[1], Xuewei Wang[2], Jonathon P. Sens[1,3], Jeanne-Pierre Kocher[2], Leonard Petrucelli[1], and John D. Fryer[1,3]

Alzheimer's disease (AD) is an age-associated neurodegenerative disease characterized by amyloidosis, tauopathy, and activation of microglia, the brain resident innate immune cells. We show that a RiboTag translational profiling approach can bypass biases due to cellular enrichment/cell sorting. Using this approach in models of amyloidosis, tauopathy, and aging, we revealed a common set of alterations and identified a central APOE-driven network that converged on CCL3 and CCL4 across all conditions. Notably, aged females demonstrated a significant exacerbation of many of these shared transcripts in this APOE network, revealing a potential mechanism for increased AD susceptibility in females. This study has broad implications for microglial transcriptomic approaches and provides new insights into microglial pathways associated with different pathological aspects of aging and AD.

Introduction

Alzheimer's disease (AD) is the leading form of dementia, marked by key pathological features of extracellular amyloid plaque deposition and intracellular neurofibrillary tangles composed of hyperphosphorylated tau (Holtzman et al., 2011). Aging is a major AD risk factor, and AD is disproportionally prevalent in females (Riedel et al., 2016). Microglia, the central nervous system (CNS)–resident innate immune population, are central cellular mediators during homeostasis and disease (Davalos et al., 2005; Nimmerjahn et al., 2005; Saijo and Glass, 2011; Nayak et al., 2014). Illuminating microglial transcriptome alterations during disease conditions is critical since genome-wide association studies have also identified several human genetic AD risk alleles that likely modulate microglial function including *CR1*, *CD33*, *TREM2*, and *APOE* (Corneveaux et al., 2010; Guerreiro et al., 2013; Liu et al., 2013; Efthymiou and Goate, 2017). Significant shifts in microglial sensome transcripts in aging and those that delineate a subpopulation of disease-associated microglia in aging and amyloidosis have been observed (Hickman et al., 2013; Keren-Shaul et al., 2017). Understanding how aging, amyloidosis, and tauopathy shape microglial transcriptomes and whether commonalities exist is critical to understanding how these factors may converge to exacerbate AD.

Results and discussion

We hypothesized that microglial cellular isolation strategies may introduce unwanted bias, as has recently been reported for muscle stem cell populations (Davalos et al., 2005; Nayak et al., 2014; van den Brink et al., 2017). We therefore explored the use of the RiboTag translational Cre/Lox-based profiling system for microglial transcript isolation based on expression of a hemagluttanin (HA) epitope-tagged core ribosomal protein (RPL22) in a cell type of interest. A tamoxifen-inducible *Cx3cr1* promoter for Cre and enhanced YFP (eYFP) expression (*Cx3cr1-Cre^{ERT2}-IRES-eYFP*; Parkhurst et al., 2013) was crossed to RiboTag mice to generate double heterozygous *Cx3cr1*$^{CreERT2\text{-}IRES\text{-}eYFP/+}$; *Rpl22*$^{HA/+}$ mice (referred to as RiboTag), to rapidly extract microglial transcripts without the necessity of cellular isolation (Fig. 1, A and B; Sanz et al., 2009; Parkhurst et al., 2013). In this approach, all mice are haploinsufficient for *Cx3cr1*, but this did not cause any general overt behavioral or cognitive phenotypes (Fig. S1, A–H).

Comparison of RiboTag versus cell enrichment with sorting (referred to generally here as "cellular isolation") methodologies for microglial transcript isolation was conducted in tamoxifen injected RiboTag mice, which induced *Cx3cr1*-YFP^{+}-HA^{+} cells (Fig. S1 I; Parkhurst et al., 2013). For the RiboTag method, mice were perfused with PBS, and forebrain tissue was immediately dispersed by brief sonication in cycloheximide-supplemented

[1]Department of Neuroscience, Mayo Clinic, Jacksonville, FL; [2]Department of Health Sciences Research, Mayo Clinic, Rochester, MN; [3]Neurobiology of Disease Graduate Program, Mayo Clinic Graduate School of Biomedical Sciences, Jacksonville, FL.

Correspondence to John D. Fryer: fryer.john@mayo.edu; Silvia S. Kang: kang.silvia@mayo.edu.

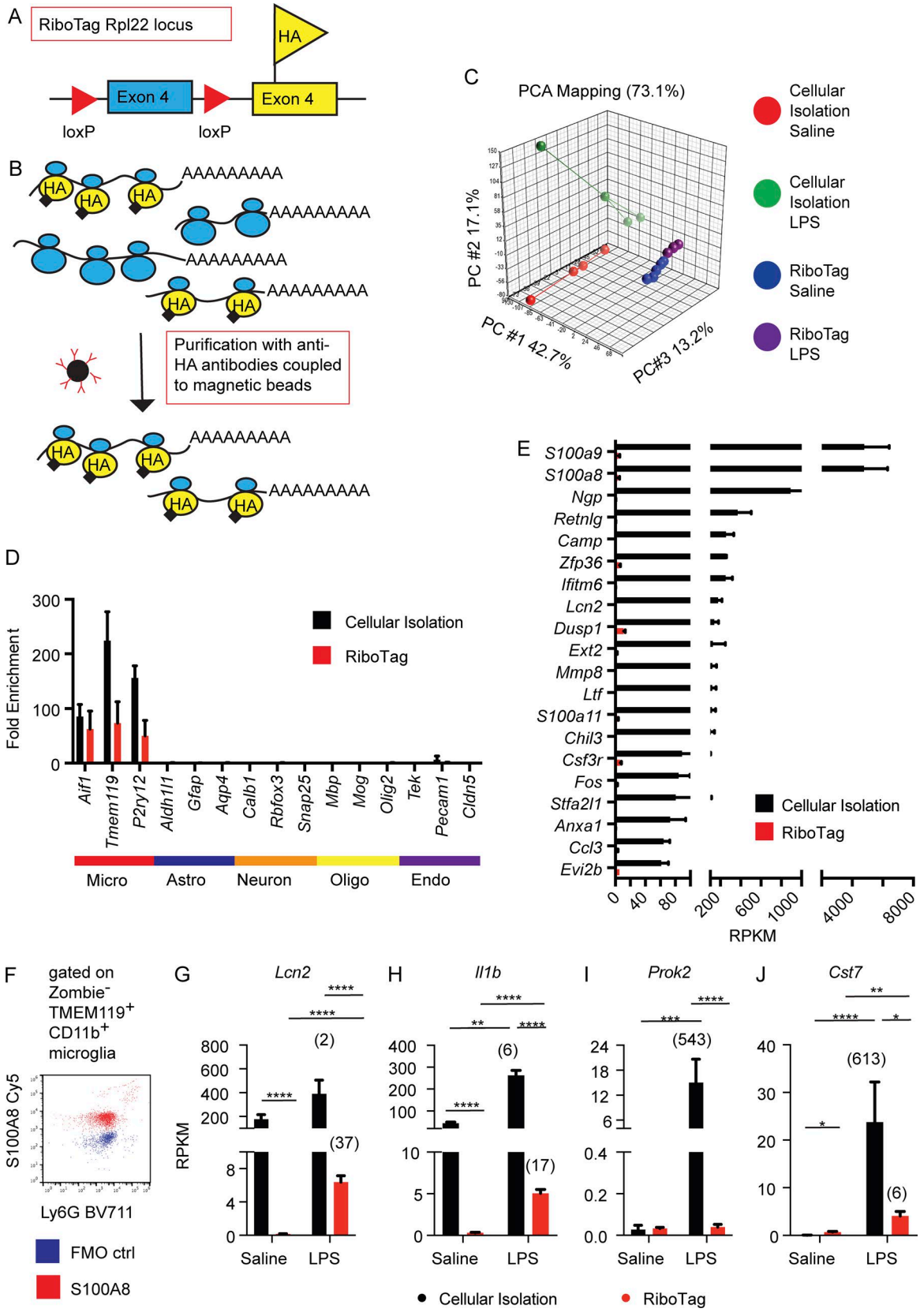

Figure 1. **Transcript isolation methodology can introduce bias in microglial transcriptomes. (A)** *Rpl22*^{HA} RiboTag model expressing an alternative HA epitope tagged *Rpl22* exon 4. **(B)** Cell-type specific promoter driven Cre expression uniquely express HA-tagged RPL22 for mRNA transcript purification at "time zero" without necessity for cellular purification. **(C)** Tamoxifen-treated *Cx3cr1*$^{CreERT2\text{-}IRES\text{-}eYFP/+}$; *Rpl22*$^{HA/+}$ mice were injected with saline or 2 mg/kg LPS i.p. and harvested at 24 h for generation of microglial RNAseq of mRNA purified by RiboTag or by cellular isolation by enzymatic digestion, Percoll gradient myelin removal, staining, and flow cytometric sorting forlive 7AAD^{-} CD11b^{+} CD45$^{lo/int}$ microglia. PCA of microglial RNAseq transcriptomes with centroids. *n* = 3–4 per

buffer to stabilize polysomes for microglial mRNA isolation using anti-HA antibody and magnetic bead purification (Doyle et al., 2008; Sanz et al., 2009). To control for drug and genotype effects, PBS-perfused forebrains from tamoxifen-injected RiboTag mice were used for cellular isolation that underwent enzymatic digestion, Percoll gradient myelin removal, staining, and flow cytometric sorting for the live 7AAD$^-$ CD11b$^+$ CD45$^{lo/int}$ microglial population to >98% (Fig. S1 J). We used these markers since they, or CD11b bead-based purification, have been widely used for microglial profiling studies. We also compared the RiboTag method to cellular isolation during robust microglial activation induced by acute peripheral lipopolysaccharide (LPS) challenge (Erickson and Banks, 2011; Kang et al., 2018). Injection of 2 µg/g LPS i.p. resulted in early inflammation followed by microglial morphological changes and activation at 24 h after injection (Fig. S1, K–N). The four RNAseq microglial transcriptome groups (RiboTag-saline, RiboTag-LPS, Cellular Isolation–saline, and Cellular Isolation–LPS) were analyzed with a false discovery rate (FDR) set at q < 0.1 and absolute fold change (FC) > 1.25 as analysis cutoffs. Principle component analysis (PCA) demonstrated that principle component 1 of transcript isolation methodology dictated the majority of the variability, even more so than LPS stimulation (Fig. 1 C). Comparison of the top 25 transcripts enriched (reads per kilobase per million mapped reads [RPKM] > 10-fold higher over input) in microglia and ranked by abundance according to RiboTag transcriptomes demonstrated that RiboTag-defined transcripts were also highly enriched in the cellular isolation dataset, validating the RiboTag method (Fig. S1 O). Additionally, transcripts associated with microglia, but not other CNS cells, were robustly enriched from input samples using both methodologies (Fig. 1 D). Comparison of baseline (saline) datasets yielded many profound differences, with 289 transcripts that were >10-fold higher in the cellular isolation dataset compared with the RiboTag dataset, 61 of which were >100-fold higher, including *S100a8*, *S100a9*, *Ngp*, *Retnlg*, *Ifitm6*, *Lcn2*, and *Mmp8* (Fig. 1 E). These transcripts may reflect a bias due to microglial activation and/or contaminating non-microglial CD45$^+$CD11b$^+$ cells such as neutrophils that could express these transcripts. However, aspects of cellular isolation procedures alone resulted in *S100a8*, *Ngp*, and *Lcn2* up-regulation that was not entirely attributed to neutrophil contamination (Fig. S2, A–H). Flow cytometry revealed distinct S100A8 expression in cellular isolated TMEM119$^+$ microglia (Fig. 1 F), in agreement with studies of activation-associated *S100a8* and *S100a9* expression in peripheral immune cells (Vogl et al., 2007; Austermann et al., 2014). Following in vivo LPS challenge, striking discrepancies in cellular isolation versus RiboTag responses were revealed by both PCA analysis (Fig. 1 C) and by the sparse overlap between the top 25 most LPS–up-regulated transcripts ranked by fold induction (Fig. S2, I and J). For some transcripts such as *Lcn2* and *Il1b*, cellular isolation elicited tremendous basal transcript expression that dampened the overall magnitude of the LPS response (Fig. 1, G and H; Kang et al., 2018). Other transcripts such as *Prok2* and *Cst7*, appeared to have a "two-hit" effect where cellular isolation in combination with LPS challenge resulted in an exaggerated response (Fig. 1, I and J). Therefore, to avoid potential skewing of the microglial transcriptomes, we used the RiboTag method to study microglial changes in mouse models of AD and normal aging.

To this end, we generated three datasets using mice on a RiboTag background that included: aging, amyloidosis (APP/PS1), and tauopathy (AAV-Tau^{P301L}; see Materials and methods for further model system details). Although the APP/PS1 and the AAV-Tau^{P301L} are overexpression systems, both provide insights regarding the two key pathological features of human AD: amyloidosis and tauopathy. Additionally, both rely on the expression of mutated forms of either the *APP* or *MAPT* gene, which were identified in humans, to initiate pathological disease. We set an FDR of q < 0.1, and absolute FC > 1.25 for all RNAseq studies. Distinct microglial transcriptomes shifts were observed by PCA during aging, amyloidosis, and tauopathy (Fig. 2, A–C). Additionally, two examples of acute inflammation, induced by either systemic injection of LPS or polyinosinic:polycytidylic acid (poly(I:C)), also showed distinct shifts in the microglial transcriptomes relative to saline controls (Fig. 2, D and E). The top 100 up-regulated transcripts sorted by aging (Fig. 2 F), amyloidosis (Fig. 2 G), and tauopathy (Fig. 2 H), revealed a striking pattern where aging had a >75% overlap in the top 100 amyloidosis and tau induced genes. Although significant shifts in the microglial transcriptome were observed with acute insults induced by LPS and poly(I:C) challenge, there was virtually no overlap with amyloidosis and tauopathy in the top 100 transcripts induced in these conditions (Fig. 2, I and J); however, within these acute inflammatory insult paradigms, LPS and poly(I:C) shared several transcripts and pathways as well as induction of unique genes (Fig. S3). Surprisingly, we found a significant amount of overlap between aging effects and LPS and poly(I:C) conditions (Fig. 2, I and J). Overall, these data indicated that aging appears to encompass aspects of both chronic and acute insults, suggesting that it could exacerbate inflammation induced with both types of neuroinflammation.

Further examination of shared transcripts suggests that tauopathy shares a common signature with aging and amyloidosis such as up-regulation of *Cst7*, *Itgax*, *Gpnmb*, *Clec7a*, *Lpl*, and *Lgals3* (Fig. 3, A–C), along with *Apoe* and *Spp1*. In models of amyloidosis, the protein encoded by targets, such as *Cst7*, *Lpl*, and *Itgax*, have been observed in amyloid associated microglia by immunofluorescence, suggesting that specific subpopulations

group from one independent experiment. **(D)** Fold enrichment of RiboTag and cellular isolation methods relative to input by RNAseq for microglial (micro; red), astrocytes (astro; blue), neurons (neuron; orange), oligodendrocytes (oligo; yellow), and endothelial (endo; purple) transcripts. Shown are the averages ± SEM, *n* = 3–4 per group from one independent experiment. **(E)** Top 20 most abundant microglial transcripts enriched in cellular isolation (>10-fold enriched over input) with >10-fold overexpression relative to RiboTag transcripts shown as averages ± SEMwith FDR set at q < 0.1. *n* = 3–4 per group from one independent experiment. **(F)** Flow plot of TMEM119$^+$ CD11b$^+$ Live Zombie$^-$ microglia with S100A8 (red) or fluorescence minus one control (FMO ctrl; blue). *n* = 3 per group, two independent experiments. **(G–J)** Average RPKM value ± SEM from RNAseq. *n* = 3–4 per group, one independent experiment for *Lcn2* (G), *Il1b* (H), *Prok2* (I), and *Cst7* (J), two-way ANOVA with Tukey posthoc *t* tests. *, P < 0.05; **, P < 0.01; ***, P < 0.001; ****, P < 0.0001. Numbers in parentheses indicate fold induction.

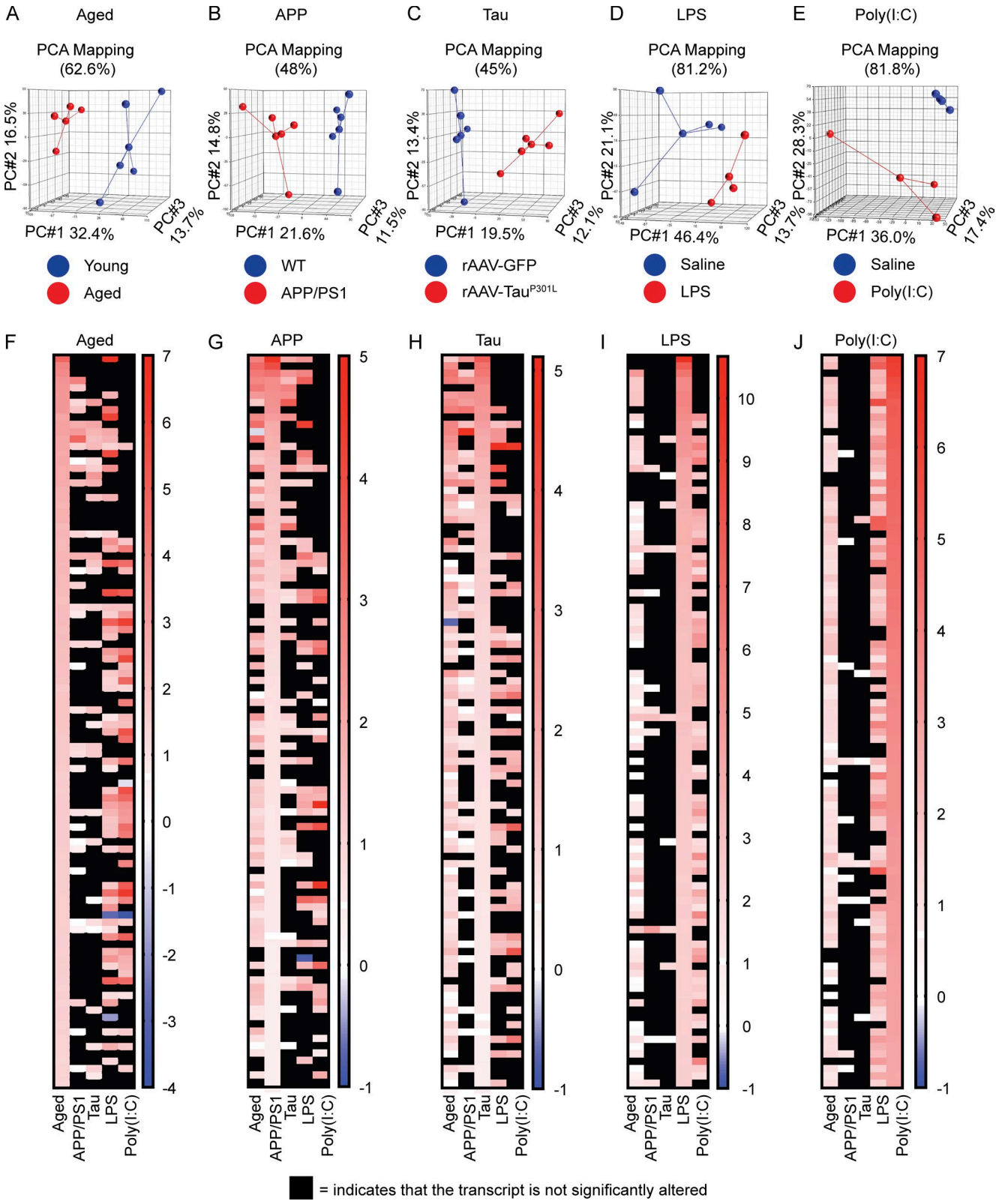

Figure 2. **Translational ribosomal profiling of microglial transcriptomes reveals amyloidosis and tauopathy responses overlap with aging but are mostly distinct from acute inflammation.** RiboTag derived microglial transcripts from aged (24-mo-old) mice, 9–10-mo-old APP/PS1, and 9–10-mo old rAAV-Tau^{P301L} Tau male mice were examined by RNAseq. **(A–E)** PCA with centroids of RNAseq datasets of microglial transcriptomes from either aged (A), APP/PS1 (B), rAAV-Tau^{P301L} (C), 2 mg/kg LPS-injected mice 24 h after challenge (D), and 12 mg/kg poly(I:C)-injected mice 24 h after challenge (E) versus controls were generated from n = 3–5 animals per group, one independent experiment. **(F–J)** Top 25 changes in microglial transcripts (FDR q < 0.1; FC > 1.25) ranked by age (F), APP/PS1 (G), Tau (H), LPS (I), and poly(I:C) (J). Scale on heat map is log2 fold change n = 3–5 animals per group, one independent experiment. Black boxes indicate that the transcript did not meet the cutoff of q < 0.1 and absolute FC ≥ 1.25.

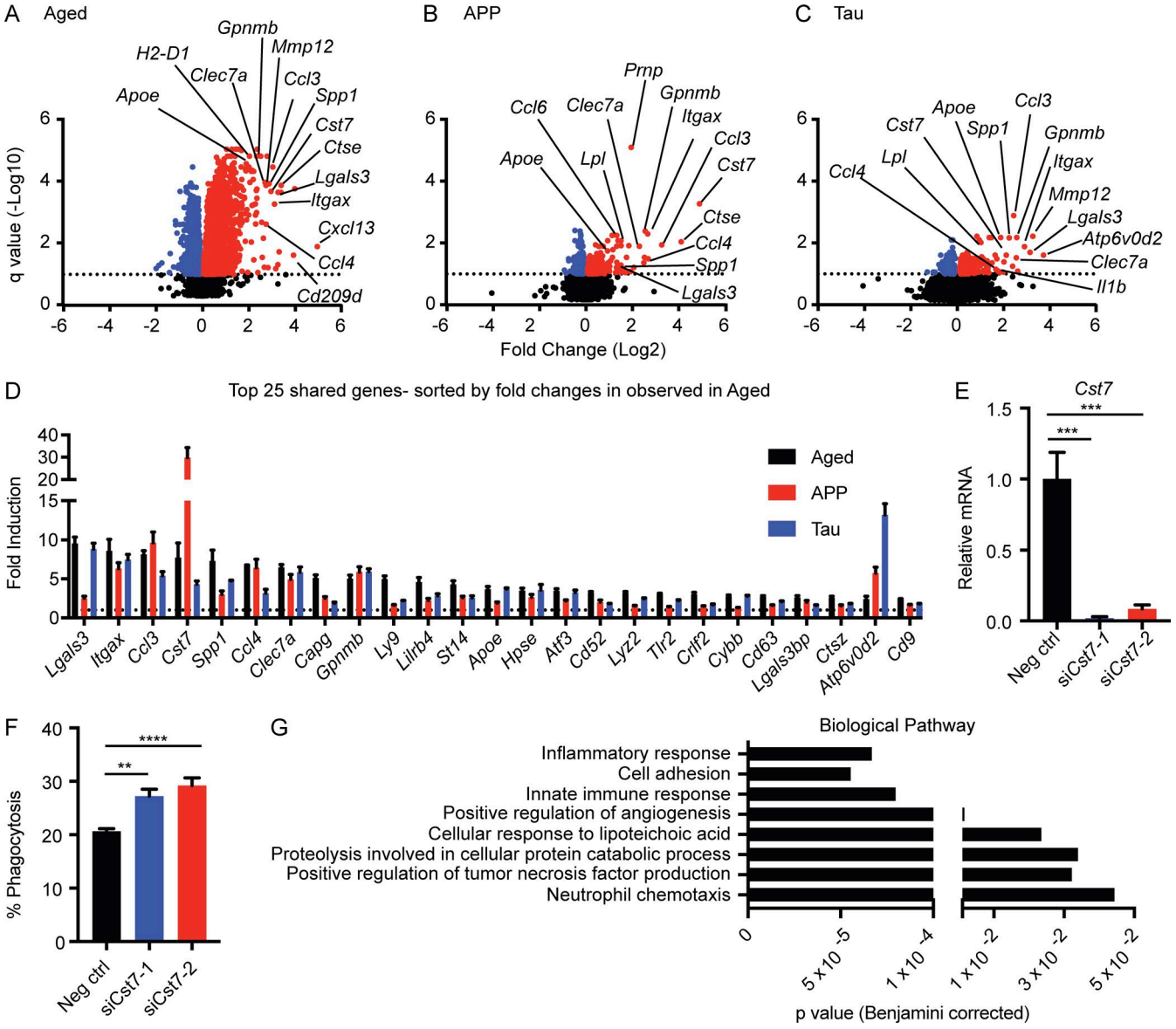

Figure 3. **Microglial transcripts shared between aging, amyloidosis, and tauopathy form significant biological pathways.** Volcano plots of microglial RiboTag isolated transcripts altered in aged (24 mo old; A), APP/PS1 (B), and rAAV-Tau^{P301L} (C). Red are FC values > 0; blue are FC values < 0. Black are transcripts that did not reach significance. The dashed lines indicate an FDR q > 0.1 (considered nonsignificant) based on n = 4–5 animals per group, one independent RNAseq experiment. **(D)** The fold up-regulation of the top 25 shared genes, sorted by the aged dataset, as averages ± SEM (n = 4–5 per group, one independent experiment). Dashed line, fold change of 1 (no change). **(E)** *Cst7* expression following *Cst7* siRNA mediated knockdown. Shown are averages ± SEM (n = 4 per group). Three independent experiments were performed. **(F)** Fluorescent sphere phagocytosis by primary microglia with siRNA mediated *Cst7* knockdown compared with control siRNA. Shown are averages ± SEM (n = 4 per group); **, P < 0.01; ***, P < 0.001; ****, P < 0.0001 by one-way ANOVA, Tukey's posthoc. Three independent experiments were performed. **(G)** Significant biological pathways by gene ontology (DAVID; NIAID/NIH) for shared microglial transcripts between aging, amyloidosis, and tauopathy.

of microglia may express these transcripts (Keren-Shaul et al., 2017; Ofengeim et al., 2017). Examination of shared genes demonstrated that *Cst7*, the most up-regulated gene during amyloidosis, was also significantly induced across all conditions. Primary microglial cultures with siRNA knockdown of *Cst7* demonstrated a significant increase in phagocytic activity (Fig. 3, E and F), suggesting that *Cst7* induction in microglial cells may contribute to the decreased phagocytic activity observed during amyloidosis, tauopathy, or aging (Krabbe et al., 2013; Keren-Shaul et al., 2017; Koellhoffer et al., 2017; Salter and Stevens, 2017).

Surprisingly, *Ccl3* and *Ccl4* emerged as significant hits within the top transcripts shared across all three conditions (Fig. 3, A–D). Since we demonstrated that *Ccl3* is prone to induction by cellular isolation (Fig. 1), this may have masked its relative importance in other studies. When examining the abundance of several shared transcripts, we found that *Ccl3* is highly abundant and falls within the top 79.7, 94.8, and 88.8% of microglial transcripts expressed in aging, amyloidosis, and tauopathy, respectively, but was low in young, WT mice. Further, of the eight significant biological pathways shared between amyloid, tau,

and aging, *Ccl3* and *Ccl4* were present in most of these, including inflammatory response (*C3ar1*, *Cybb*, *Ccl3*, *Crl2*, *Axl*, *Tlr2*, *Clec7a*, *Ccl4*, *Cd14*, and *Spp1*), positive regulation of tumor necrosis factor production (*Ccl3*, *Tlr2*, *Ccl4*, and *Cd14*), and neutrophil chemotaxis pathways (*Ccl3*, *Lgals3*, *Ccl4*, and *Spp1*; Fig. 3 G). Interestingly, CNS neutrophil recruitment/extravasation has been shown to exacerbate pathology and cognitive impairment in AD models (Baik et al., 2014; Zenaro et al., 2015). Additionally, sepsis, which can result in CNS neutrophil recruitment, has also been associated with cognitive decline (Iwashyna et al., 2010; He et al., 2016). These data suggest that *Ccl3* and *Ccl4* may be integral in microglial function in aging and disease, potentially through CNS recruitment of neutrophil or other peripheral immune cells

Though not a microglia-specific gene, the absolute abundance of *Apoe* even under basal conditions places it in the top 99% of all transcripts expressed in microglia, even higher than known microglial marker genes such as *Tmem119*, *Trem2*, *Cx3cr1*, or *Aif1*, the gene encoding IBA1 (Fig. 4, A–D). Examination of *Apoe* revealed that it was significantly up-regulated in aging, amyloidosis, and tauopathy (Fig. 4, E–G). Strikingly, Ingenuity pathway analysis of shared microglial transcripts observed in these three conditions revealed a strong APOE-driven network that converged on CCL3 and CCL4 (Fig. 4 H). Recent work examining *Apoe*$^{-/-}$ mice in an amyloidosis model demonstrated decreased *Ccl3* and *Ccl4* transcripts and hippocampal CCL3 protein levels (Ulrich et al., 2018). Additionally, examination of TMEM119^{+}CD11b^{+} microglia from *Apoe*$^{-/-}$ mice revealed a significant decrease in SPP1, a gene up-regulated across all conditions and present in the APOE network (Fig. 4, H and I). Collectively, these data suggest a significant in vivo effect of APOE expression on this network. Although APOE is known to contribute to disease through many mechanisms and can exacerbate both amyloidosis and tauopathy (Liu et al., 2013; Shi et al., 2017), the role of microglial APOE and whether it serves a unique or redundant role with astrocyte APOE is unknown.

In addition to aging, sex is another AD risk factor. Previous microarray analysis revealed age-related sexually divergent neuroinflammatory and complement genes in bulk hippocampal tissue (Mangold et al., 2017). To determine how sex affects the aged microglial transcriptome, we compared RiboTag RNA-seq microglial transcriptomes from 3-, 12-, and 24-mo-old male and female mice. PCA analysis revealed discrete populations that separated most by the principle component 1 aspect of aging (Fig. 5 A) with the majority of sex differences occurring at 24-mo of age (Fig. 5, B–D). A potential caveat is that the sample sizes for RNAseq was *n* of four to five samples per group; therefore, it is possible that additional transcripts would be significant if we had even higher numbers to provide additional statistical power. This may account for the low number of significant differences between sexes, especially at earlier ages. Notably, in both sexes the middle-age samples appeared to have an intermediate transcript up-regulation (Fig. 5 E), suggesting a gradual shift in the transcriptome. Surprisingly, of the 37 transcripts that were significantly altered between 24-mo-old females and males ($q < 0.1$, absolute FC > 1.25), seven (18.9%) of the transcripts were found in the APOE driven network (Fig. 4 H) with significantly higher expression of *Spp1*, *Gpnmb*, *Lgals3*, *Apoe*, *Ccl3*, *Clec7a*, and *Ccl4* in females (Fig. 5 F). This suggests that this network may be critical for driving the increased susceptibility of aged females at basal states and in the context of neurodegeneration.

Collectively, our results suggest that the risk factors of aging and sex, along with the pathological features of amyloidosis and tauopathy, serve to induce a core set of microglial transcripts that drive an APOE-mediated response resulting in CCL3 and CCL4 production. Although astrocyte-derived APOE has remained a large focus of AD related APOE research, our data suggest that microglial-derived APOE may also play a significant role in disease. Additionally, the overwhelming convergence of this core set of transcripts indicates that these multiple "hits" together may significantly exacerbate microglial dysfunction, resulting in increased pathology through these key mediators that could be critical targets for future therapeutics.

Materials and methods

Animals

C57BL/6J, APPswe/PS1ΔE9 (APP/PS1)[29], and *Cx3cr1-Cre*^{ERT2}-*IRES-eYFP*$^{+/-}$; Rpl22$^{HA/+}$ mice (The Jackson Laboratory) were housed under standard laboratory conditions in ventilated cages on 12-h light:dark cycles in a specific pathogen-free environment. To generate the *Cx3Cr1*creER; Rpl22 mice, two independent strains both on a C57BL/6J background derived from The Jackson Laboratory, the Cx3Cr1$^{tm2.1(Cre/ERT2)}$ and Rpl22$^{tm1.1PSam}$ were bred and used as heterozygous mice for all studies (i.e., *Cx3Cr1*$^{creER/+}$; Rpl22$^{HA/+}$). For LPS and poly(I:C) studies, animals were injected with 2 µg/g LPS (0111:B4; Sigma) or 12 µg/g poly(I:C) (HMW; Invivogen) i.p., respectively. To induce tagged RPL22 expression, 3–4-mo-old male *Cx3Cr1*$^{cre/+}$; Rpl22$^{HA/+}$ mice were injected for three consecutive days with 100 µg/g tamoxifen (Sigma). 9–10-mo-old male APPswe/PS1ΔE9 (APP/PS1) and littermate controls were used for RNAseq studies. Animal protocols were reviewed and approved by Mayo Clinic Institutional Animal Care and Use Committee.

rAAV-GFP and rAAV-Tau^{P301L} injections

Cx3Cr1$^{creER/+}$; Rpl22$^{HA/+}$ pups were injected intracerebroventricularly with 2.7E + 10 viral particles/ventricle and 2 µl/ventricle of rAAV1-Tau^{P301L} and rAAV1-GFP on postnatal day 0. Viral production and injections were performed as described (Cook et al., 2015). In brief, cryoanesthetized newborn mice were placed on a cold metal plate, and a 30-G needle was used to pierce the skull just posterior to bregma and 2 mm lateral to the midline. For each lateral ventricle, 2 µl of AAV was injected, before rewarming the pups. Male animals were aged to 9–10 mo and used for RNAseq studies.

Tissue processing

Animals were deeply anesthetized with pentobarbital before cardiac perfusion with PBS to expunge blood from the cerebrovasculature. For biochemical analysis, forebrain tissues were quickly dissected, frozen on dry ice, and stored at −80°C until further processing. Tissues set aside for immunohistochemistry were prepared as indicated below.

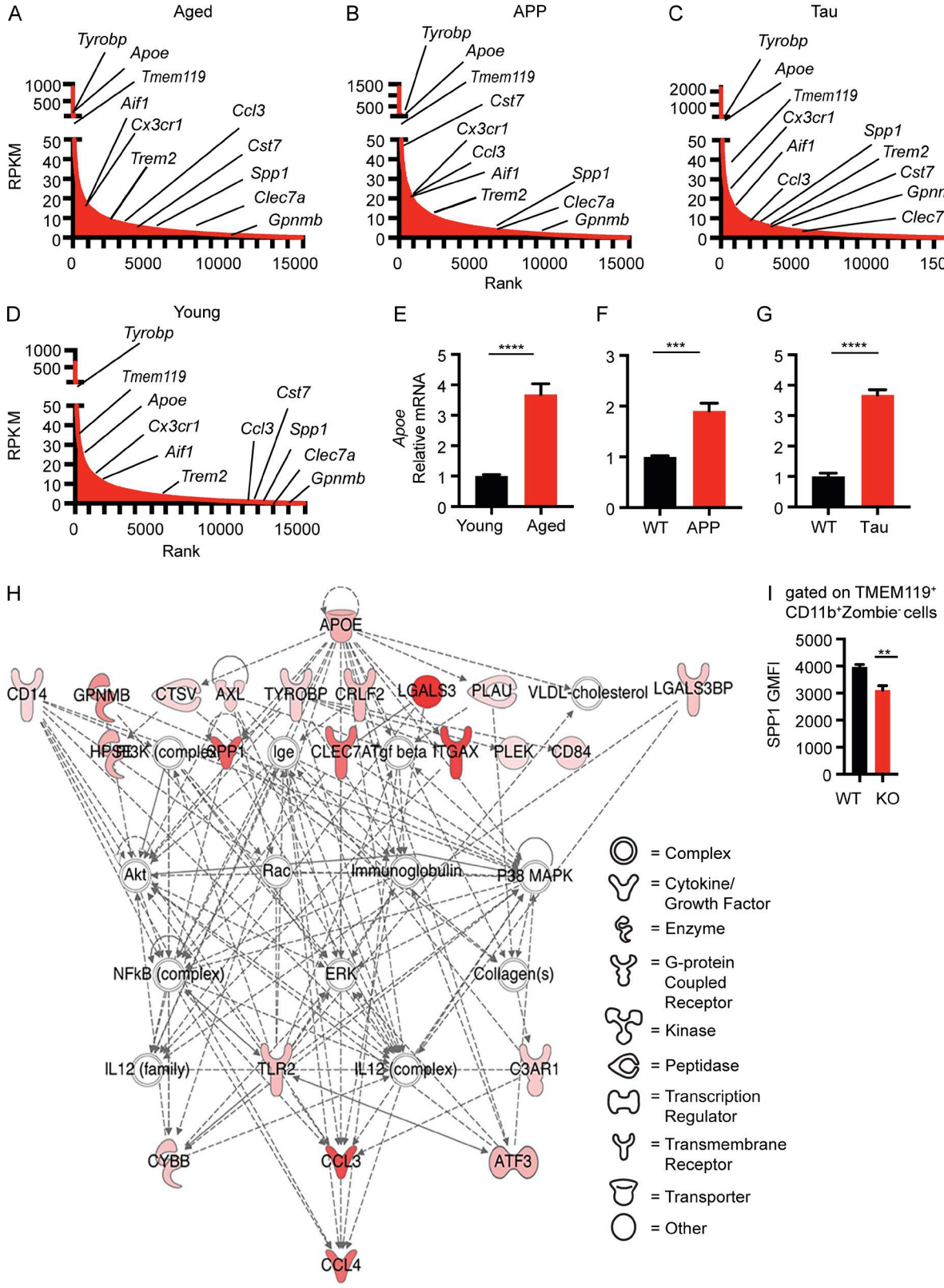

Figure 4. **Microglial APOE drives the top network formed by shared microglial transcripts between aging, amyloidosis, and tauopathy. (A–D)** RPKM versus abundance ranking of microglial transcripts in aged (24 mo old; A), APP/PS1 (B), Tau (C), and young 3-mo-old males (D) based on n = 4–5 animals per group, one independent RNAseq experiment. **(E–G)** Relative *ApoE* microglial mRNA up-regulation in aged (24 mo old; E), APP (F), and Tau (G) versus respective controls. Shown are averages ± SEM (n = 4–5 per group, one independent experiment); ***, P < 0.001, ****, P < 0.0001 by unpaired two-tailed Student's t test. **(H)** Ingenuity network analysis of the shared transcripts between aging, amyloidosis, and tauopathy with FDR set at q < 0.1 and absolute FC > 1.25. **(I)** SPP1 geometric mean fluorescence intensity (GMFI) by flow cytometric analysis of live TMEM119^{+}CD11b^{+} microglia between WT and *Apoe*$^{-/-}$ mice shown as averages ± SEM; **, P < 0.01 unpaired two-tailed Student's t test, n = 3–5 animals per group, two independent experiments.

RNA extraction for qPCR

For RNA extraction of tissues, frozen forebrains were briefly sonicated in Tris buffered saline with EDTA (TBSE; 50 mM Tris, pH 7.5, 150 mM NaCl, and 1 mM EDTA) with 1× protease and phosphatase inhibitors (Thermo-Fisher Scientific). An aliquot of the tissue suspension was processed for RNA. For RNA extraction of cells isolated using myelin beads or Percoll methodologies, cells were pelleted at the final step and lysed in RLT Lysis Plus buffer supplemented with β-mercaptoethanol. Total RNA was isolated from tissues using an RNeasy Plus micro isolation kit according to manufacturer's instructions (Qiagen).

Real-time quantitative PCR (qRT-PCR)

Random-primed reverse transcription was performed according to manufacturer protocols (Invitrogen; Life Technologies). cDNA was added to a reaction mix (10-µl final volume) containing 300 nM gene-specific primers and Universal SYBR green supermix (Bio-Rad). All samples were run in triplicate and were analyzed on a Quant Studio 7 Flex Real Time PCR instrument (Applied Biosystems; Life Technologies). Relative gene expression was normalized to GAPDH controls and assessed using the $2^{-\Delta\Delta CT}$ method. Primer sequences are as follows (5′ to 3′): *Gapdh* F: CTG CACCACCAACTGCTTAG, *Gapdh* R: ACAGTCTTCTGGGTGGCAGT; *Aif1*(Iba1) F: GGATTTGCAGGGAGGAAAAG, *Aif1*(Iba1), R: TGGGAT CATCGAGGAATTG; *Il1b* F: CCTGCAGCTGGAGAGTGTGGAT, *IL1b* R: TGTGCTCTGCTTGTGAGGTGCT; *Tnfa* F: AGCCCACGTCGTAGC AAACCAC, *Tnfa* R: AGGTACAACCCATCGGCTGGCA; *S100a8* F: CCTTTGTCAGCTCCGTCTTC, *S100a8* R: CAAGGCCTTCTCCAG TTCAG; *Ngp* F: CTCTTCCGCCTGCTAAGTG, *Ngp* R: TGAACTGGA GTGGGATATTGG; *Lcn2* F: ATGTCACCTCCATCCTGGTC, *Lcn2* R: CCTGGAGCTTGGAACAAATG.

Immunohistochemistry

PBS-perfused hemi-brains were drop fixed into 10% neutral-buffered formalin (Thermo-Fisher Scientific) overnight at 4°C. Tissue was then placed in 30% sucrose (Sigma) dissolved in PBS overnight at 4°C. 50-µm coronal brain sections were cut on a freezing-sliding microtome and stored in cryoprotectant at −20°C until staining. Sections were blocked for endogenous peroxidase activity and permeabilized with 0.6% H_2O_2 and 0.1% NaN_3 in PBS-X (1× PBS containing 0.3% Triton-X) for 30 min at room temperature. Sections were blocked with 1% milk in PBS-X followed by incubation with rabbit anti-IBA1 at 1:8,000 (019-9741; Wako) in 0.5% milk PBS-X for 2 d at 4°C. Sections were then incubated with the Vectastain kit anti-rabbit IgG (Vector Labs) overnight at 4°C followed by ABC component for 4 h and developed using the DAB kit (Vector Labs) according to manufacturer's instructions. Images were acquired using an XT Scanner (Aperio) at a 20× magnification.

Cell sorting of microglia and RNA extraction for RNAseq

PBS-perfused brains from tamoxifen injected *Cx3Cr1*$^{creER/+}$; Rpl22$^{HA/+}$ mice challenged with either saline or 2 µg/g LPS i.p. were incubated with collagenase D for 20 min at 37°C. Brains were immediately disrupted into a single cell suspension, filtered through a 100-µm filter, and washed with HBSS. Samples were centrifuged for 5 min at 300 *g*. Supernatants were aspirated and the cell pellet was resuspended in 90% Percoll/1× HBSS. A Percoll gradient was made with additional layers of 60% Percoll/1× HBSS, 40% Percoll/1× HBSS, and HBSS. Gradients were centrifuged for 18 min at 500 *g* with no brake, and cells were isolated from the 60/40 interface. Cells were washed twice with HBSS, incubated with Fc block for 10 min on ice in 1% BSA/HBSS buffer, and then stained for 30 min with anti-CD11b PE/Cy7 and anti-CD45 APC (Biolegend). Cells were sorted using 7AAD$^-$ CD11b$^+$ CD45$^{lo/int}$ as the gate to identify microglia, and sorted directly into a 1.5-mL microcentrifuge tube containing Buffer RLT using a FACS Aria II SORP (BD Bioscience). RNA was extracted using a Qiagen RNeasy Microkit (Qiagen). This process from brain extraction to sorting into a microcentrifuge tube was ∼4 h.

RiboTag microglial RNA isolation

Cx3Cr1$^{cre/+}$; Rpl22$^{HA/+}$ mice were injected for three consecutive days with 100 µg/g tamoxifen (Sigma) resuspended in corn oil to induce nuclear localization of CreER and allow for HA-tagged Rpl22 expression. 1 wk following the final injection, animals were challenged i.p. either with saline or 2 µg/g LPS. At 24 h after injection, animals were anesthetized with pentobarbital and PBS-perfused before forebrain harvest and immediate tissue sonication in homogenization buffer (50 mM Tris, pH 7.4, 100 mM KCl, 12 mM $MgCl_2$, and 1% NP-40) supplemented with 1 mM DTT, 1× protease/phosphatase inhibitors (Thermo-Fisher Scientific), 200 U/ml RNAsin, 100 µg/ml cycloheximide, and 1 mg/ml heparin. The cycloheximide serves to stabilize mRNA onto ribosomal complexes(Doyle et al., 2008; Sanz et al., 2009). A portion of this was immediately added to buffer RLT and RNA was purified to serve as "input" for each sample. Lysates were centrifuged at 4°C at 10,000 *g* for 10 min. Supernatants were incubated with anti-HA antibodies (Biolegend) and rotated at 4°C for 4 h before addition of protein G magnetic beads (Bio-Rad) and overnight incubation at 4°C while rotating. Beads were magnetized and non-HA containing supernatants were removed before washing with a high salt buffer (50 mM Tris, 300 mM KCl, 12 mM $MgCl_2$, 10% NP-40, 1 mM DTT, and 100 µg/ml cycloheximide). Three washes were conducted before magnetizing the beads, removing all supernatants and then releasing HA bound transcripts from the beads using Buffer RLT supplemented with 2-β-mercaptoethanol from a (Qiagen) RNeasy microkit followed by in-column DNase I treatment and isolation of RNA according to manufacturer's instructions. Samples were amplified for RNAseq by cDNA library preparation using a NuGen Ovation RNA v2 kit (NuGen).

Illumina RNA sequencing and pathway analysis

All samples were sequenced at Mayo Clinic Genome Facility using an Illumina HiSeq 4000. Reads were mapped to the mouse genome mm10 and RPKM were generated for each transcript. RPKM values were log2 transformed, and low abundance transcripts were removed from further analysis (log2 RPKM > −2 across all experimental groups were considered too lowly expressed). Differential expression, PCA, and statistical analysis were performed using Partek Genomics Suite (Partek Inc.) with ANOVA followed by multiple test comparison adjustment of P values using Bonferroni correction with FDR set at $q < 0.1$. Pathway analyses were performed using DAVID (National Institute of Allergy and Infectious Diseases) to examine significantly enriched pathways.

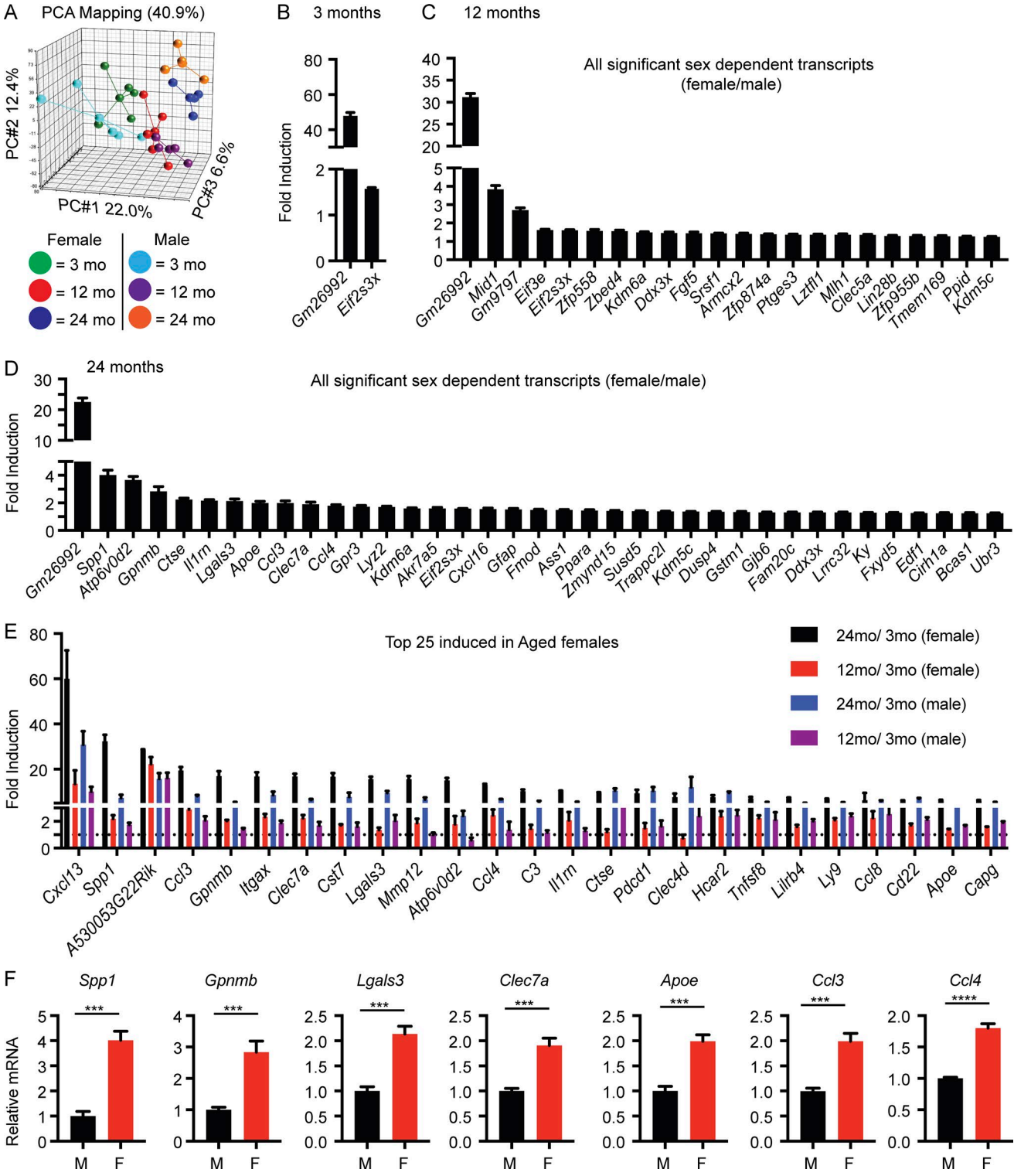

Figure 5. **Age related sex differences reveal exacerbation of numerous transcripts involved in the APOE-driven network of CCL3 and CCL4 production.** Tamoxifen injected Cx3Cr1$^{CreER/+}$; Rpl22$^{HA/+}$ ("RiboTag") male and female mice were analyzed by RNAseq at 3, 12, and 24 mo of age with FDR set at q < 0.1 and FC > 1.25. **(A)** PCA of microglial transcriptomes from 3-mo-old males and females, 12-mo-old males and females, and 24-mo-old males and females were generated from *n* = 4–5 animals per group, one independent experiment. **(B–D)** Female microglial transcripts at 3 mo (B), 12 mo (C), and 24 mo (D) that were significantly up-regulated compared with male transcripts from the corresponding age. Data are shown for each age as an average ± SEM for *n* = 4–5 mice per group, one independent experiment. **(E)** Examination of the top 25 up-regulated transcripts in aged (24-mo-old) females versus young (3-mo-old) females were shown relative to alterations observed in 12-mo versus 3-mo-old females, 24-mo versus 3-mo-old males, and 12-mo versus 3-mo-old males. Shown is the average fold up-regulation ± SEM for *n* = 4–5 mice per group, one independent RNA seq experiment. **(F)** Transcripts significantly altered by sex in aged, 24-mo-old mice, observed in the APOE-driven pathway. M is male, F is female. Bar graphs are averages ± SEM; ***, P < 0.001; ****, P < 0.0001 unpaired two-tailed Student's *t* test (*n* = 4–5 per group, one independent experiment).

Myelin bead removal

Following PBS perfusion, forebrains were removed, minced, and immediately incubated in StemPro Accutase (Thermo-Fisher Scientific) for 30 min at 4°C while rocking. Samples were centrifuged for at 4°C at 300 *g* for 10 min. The tissue pellet was resuspended in ice-cold HBSS and triturated sequentially using a 10-ml pipette, 5-ml pipette, and a P1000 pipet tip. Cells were filtered through a 100-µm strainer and then a 70-µm strainer before centrifugation at 4°C at 300 *g* for 10 min. The pellet was resuspended in 1.8 ml MACS buffer (0.5% BSA in PBS) and 200 µl myelin depletion beads were added, and depletion was conducted according to manufacturer's instructions (Miltenyi Biotec). Tissues were taken before Accutase digestion, following Accutase digestion, and after myelin removal to generate RNA using a Qiagen RNeasy micro kit (Qiagen) for RT-qPCR.

S100A8 flow cytometry

Cells isolated from PBS-perfused brains following collagenase digestion and myelin removal using a Percoll gradient were washed in HBSS. Cells were resuspended in PBS and incubated for 15 min with Zombie violet (Biolegend) at room temperature. Cells were washed with PBS and then resuspended in staining buffer (1% BSA and PBS) and blocked with Fc block with 1:100 anti-CD16/32 (Biolegend) for 15 min on ice, followed by surface staining with anti-CD11b PE/Cy7, anti-Ly6G BV711 (Biolegend), and rabbit anti-TMEM119 (Abcam) for 15 min. Cells were washed with PBS, centrifuged for 5 min at 300 *g*, and then stained Alexa Fluor 488 conjugated with donkey anti-rabbit antibody (Jackson ImmunoResearch) for 15 min on ice. Following a PBS wash and 5 min centrifugation at 300 *g*, cells were resuspended in fixation buffer (Biolegend) for 15 min at room temperature. Cells were washed with PBS and then washed with permeabilization buffer (Biolegend) three times. Goat anti-S100A8 (R&D Systems) intracellular stain was conducted for 15 min on ice. Samples were washed with permeabilization buffer and then stained with donkey anti-goat Cy5 for 15 min on ice. Following two washes, cells were resuspended in 1% BSA/PBS buffer for analysis. Samples were read on an Attune NxT (Thermo-Fisher Scientific) and analyzed using FlowJo v10 software (FlowJo).

Data and materials availability

RNAseq data are deposited in Gene Expression Omnibus database (GSE117646).

Online supplemental material

Fig. S1 shows system setup including behavioral and cognitive assessment of *Cx3cr1*$^{+/+}$, *Cx3cr1*$^{gfp/+}$, and *Cx3cr1*$^{gfp/gfp}$ animals; confocal analysis of HA expression in tamoxifen injected heterozygous *Cx3cr1*$^{CreERT2\text{-}IRES\text{-}eYFP/+}$; *Rpl22*$^{HA/+}$ mice (referred to as RiboTag in the manuscript); and cellular sorting strategies. A timecourse of LPS induced CNS inflammation to determine the time point for LPS studies is shown. The top 25 transcripts in microglia determined by RNAseq in RiboTag versus Cellular (RPKM > 10-fold higher over input) is also shown. Fig. S2 details the impact of different enzymatic conditions, myelin removal methodologies, and neutrophil depletion on activation/contamination markers. A comparison of the top LPS induced microglial transcripts determined using RNAseq data ranked according to both the cellular isolation dataset, and the RiboTag dataset 24 h after LPS challenge is also shown. Fig. S3 displays the Venn diagram of LPS and poly(I:C) induced microglial transcripts as well as the top 10 biological pathways 24 h following systemic challenge with either stimulant. The top induced transcripts based on RNAseq data ranked either using the LPS or poly(I:C) data are also shown. Supplemental material for this paper can be found at https://www.fryerlab.com/ribotag website. This content has not been peer reviewed.

Acknowledgments

This work was supported by grants from Mayo Foundation, GHR Foundation, Mayo Clinic Center for Individualized Medicine, Mayo Clinic Gerstner Family Career Development Award, Ed and Ethel Moore Alzheimer's Disease Research Program of Florida Department of Health (grant 6AZ06 to J.D. Fryer), and National Institutes of Health grants NS094137, AG047327, and AG049992 (to J.D. Fryer); MH103632 (to S.S. Kang); AG057997 and AG016574 (J.D. Fryer and S.S. Kang); NS100693, NS097273, NS084974, and NS100693 (L. Petrucelli).

The authors declare no competing financial interests.

Author contributions: S.S. Kang and J. Fryer designed all the experiments. S.S. Kang, J.P. Sens, and C. Cook performed the research. X. Wang and J.-P. Kocher performed RNAseq sequence processing. M.T.W. Ebbert assisted in RNAseq analysis and website construction. K.E. Baker provided colony breeding and maintenance for mouse studies and additional technical support. S. Kang and J.D. Fryer wrote the manuscript with input from L. Petrucelli.

Submitted: 6 April 2018
Revised: 25 June 2018
Accepted: 20 July 2018

References

Austermann, J., J. Friesenhagen, S.K. Fassl, B. Petersen, T. Ortkras, J. Burgmann, K. Barczyk-Kahlert, E. Faist, S. Zedler, S. Pirr, et al. 2014. Alarmins MRP8 and MRP14 induce stress tolerance in phagocytes under sterile inflammatory conditions. *Cell Reports.* 9:2112–2123. https://doi.org/10.1016/j.celrep.2014.11.020

Baik, S.H., M.-Y. Cha, Y.-M. Hyun, H. Cho, B. Hamza, D.K. Kim, S.-H. Han, H. Choi, K.H. Kim, M. Moon, et al. 2014. Migration of neutrophils targeting amyloid plaques in Alzheimer's disease mouse model. *Neurobiol. Aging.* 35:1286–1292. https://doi.org/10.1016/j.neurobiolaging.2014.01.003

Cook, C., S.S. Kang, Y. Carlomagno, W.L. Lin, M. Yue, A. Kurti, M. Shinohara, K. Jansen-West, E. Perkerson, M. Castanedes-Casey, et al. 2015. Tau deposition drives neuropathological, inflammatory and behavioral abnormalities independently of neuronal loss in a novel mouse model. *Hum. Mol. Genet.* 24:6198–6212. https://doi.org/10.1093/hmg/ddv336

Corneveaux, J.J., A.J. Myers, A.N. Allen, J.J. Pruzin, M. Ramirez, A. Engel, M.A. Nalls, K. Chen, W. Lee, K. Chewning, et al. 2010. Association of CR1, CLU and PICALM with Alzheimer's disease in a cohort of clinically characterized and neuropathologically verified individuals. *Hum. Mol. Genet.* 19:3295–3301. https://doi.org/10.1093/hmg/ddq221

Davalos, D., J. Grutzendler, G. Yang, J.V. Kim, Y. Zuo, S. Jung, D.R. Littman, M.L. Dustin, and W.-B. Gan. 2005. ATP mediates rapid microglial response to local brain injury in vivo. *Nat. Neurosci.* 8:752–758. https://doi.org/10.1038/nn1472

Doyle, J.P., J.D. Dougherty, M. Heiman, E.F. Schmidt, T.R. Stevens, G. Ma, S. Bupp, P. Shrestha, R.D. Shah, M.L. Doughty, et al. 2008. Application of a translational profiling approach for the comparative analysis of CNS cell types. *Cell.* 135:749–762. https://doi.org/10.1016/j.cell.2008.10.029

Efthymiou, A.G., and A.M. Goate. 2017. Late onset Alzheimer's disease genetics implicates microglial pathways in disease risk. *Mol. Neurodegener.* 12:43. https://doi.org/10.1186/s13024-017-0184-x

Erickson, M.A., and W.A. Banks. 2011. Cytokine and chemokine responses in serum and brain after single and repeated injections of lipopolysaccharide: multiplex quantification with path analysis. *Brain Behav. Immun.* 25:1637–1648. https://doi.org/10.1016/j.bbi.2011.06.006

Guerreiro, R., A. Wojtas, J. Bras, M. Carrasquillo, E. Rogaeva, E. Majounie, C. Cruchaga, C. Sassi, J.S.K. Kauwe, S. Younkin, et al. Alzheimer Genetic Analysis Group. 2013. TREM2 variants in Alzheimer's disease. *N. Engl. J. Med.* 368:117–127. https://doi.org/10.1056/NEJMoa1211851

He, H., T. Geng, P. Chen, M. Wang, J. Hu, L. Kang, W. Song, and H. Tang. 2016. NK cells promote neutrophil recruitment in the brain during sepsis-induced neuroinflammation. *Sci. Rep.* 6:27711. https://doi.org/10.1038/srep27711

Hickman, S.E., N.D. Kingery, T.K. Ohsumi, M.L. Borowsky, L.C. Wang, T.K. Means, and J. El Khoury. 2013. The microglial sensome revealed by direct RNA sequencing. *Nat. Neurosci.* 16:1896–1905. https://doi.org/10.1038/nn.3554

Holtzman, D.M., J.C. Morris, and A.M. Goate. 2011. Alzheimer's disease: the challenge of the second century. *Sci. Transl. Med.* 3:77sr1. https://doi.org/10.1126/scitranslmed.3002369

Iwashyna, T.J., E.W. Ely, D.M. Smith, and K.M. Langa. 2010. Long-term cognitive impairment and functional disability among survivors of severe sepsis. *JAMA.* 304:1787–1794. https://doi.org/10.1001/jama.2010.1553

Kang, S.S., Y. Ren, C.-C. Liu, A. Kurti, K.E. Baker, G. Bu, Y. Asmann, and J.D. Fryer. 2018. Lipocalin-2 protects the brain during inflammatory conditions. *Mol. Psychiatry.* 23:344–350. https://doi.org/10.1038/mp.2016.243

Keren-Shaul, H., A. Spinrad, A. Weiner, O. Matcovitch-Natan, R. Dvir-Szternfeld, T.K. Ulland, E. David, K. Baruch, D. Lara-Astaiso, B. Toth, et al. 2017. A Unique Microglia Type Associated with Restricting Development of Alzheimer's Disease. *Cell.* 169:1276–1290.e17. https://doi.org/10.1016/j.cell.2017.05.018

Koellhoffer, E.C., L.D. McCullough, and R.M. Ritzel. 2017. Old Maids: Aging and Its Impact on Microglia Function. *Int. J. Mol. Sci.* 18:769. https://doi.org/10.3390/ijms18040769

Krabbe, G., A. Halle, V. Matyash, J.L. Rinnenthal, G.D. Eom, U. Bernhardt, K.R. Miller, S. Prokop, H. Kettenmann, and F.L. Heppner. 2013. Functional impairment of microglia coincides with Beta-amyloid deposition in mice with Alzheimer-like pathology. *PLoS One.* 8:e60921. https://doi.org/10.1371/journal.pone.0060921

Liu, C.-C., C.-C. Liu, T. Kanekiyo, H. Xu, and G. Bu. 2013. Apolipoprotein E and Alzheimer disease: risk, mechanisms and therapy. *Nat. Rev. Neurol.* 9:106–118. https://doi.org/10.1038/nrneurol.2012.263

Mangold, C.A., B. Wronowski, M. Du, D.R. Masser, N. Hadad, G.V. Bixler, R.M. Brucklacher, M.M. Ford, W.E. Sonntag, and W.M. Freeman. 2017. Sexually divergent induction of microglial-associated neuroinflammation with hippocampal aging. *J. Neuroinflammation.* 14:141. https://doi.org/10.1186/s12974-017-0920-8

Nayak, D., T.L. Roth, and D.B. McGavern. 2014. Microglia development and function. *Annu. Rev. Immunol.* 32:367–402. https://doi.org/10.1146/annurev-immunol-032713-120240

Nimmerjahn, A., F. Kirchhoff, and F. Helmchen. 2005. Resting microglial cells are highly dynamic surveillants of brain parenchyma in vivo. *Science.* 308:1314–1318. https://doi.org/10.1126/science.1110647

Ofengeim, D., S. Mazzitelli, Y. Ito, J.P. DeWitt, L. Mifflin, C. Zou, S. Das, X. Adiconis, H. Chen, H. Zhu, et al. 2017. RIPK1 mediates a disease-associated microglial response in Alzheimer's disease. *Proc. Natl. Acad. Sci. USA.* 114:E8788–E8797. https://doi.org/10.1073/pnas.1714175114

Parkhurst, C.N., G. Yang, I. Ninan, J.N. Savas, J.R. Yates III, J.J. Lafaille, B.L. Hempstead, D.R. Littman, and W.-B. Gan. 2013. Microglia promote learning-dependent synapse formation through brain-derived neurotrophic factor. *Cell.* 155:1596–1609. https://doi.org/10.1016/j.cell.2013.11.030

Riedel, B.C., P.M. Thompson, and R.D. Brinton. 2016. Age, APOE and sex: Triad of risk of Alzheimer's disease. *J. Steroid Biochem. Mol. Biol.* 160:134–147. https://doi.org/10.1016/j.jsbmb.2016.03.012

Saijo, K., and C.K. Glass. 2011. Microglial cell origin and phenotypes in health and disease. *Nat. Rev. Immunol.* 11:775–787. https://doi.org/10.1038/nri3086

Salter, M.W., and B. Stevens. 2017. Microglia emerge as central players in brain disease. *Nat. Med.* 23:1018–1027. https://doi.org/10.1038/nm.4397

Sanz, E., L. Yang, T. Su, D.R. Morris, G.S. McKnight, and P.S. Amieux. 2009. Cell-type-specific isolation of ribosome-associated mRNA from complex tissues. *Proc. Natl. Acad. Sci. USA.* 106:13939–13944. https://doi.org/10.1073/pnas.0907143106

Shi, Y., K. Yamada, S.A. Liddelow, S.T. Smith, L. Zhao, W. Luo, R.M. Tsai, S. Spina, L.T. Grinberg, J.C. Rojas, et al. Alzheimer's Disease Neuroimaging Initiative. 2017. ApoE4 markedly exacerbates tau-mediated neurodegeneration in a mouse model of tauopathy. *Nature.* 549:523–527. https://doi.org/10.1038/nature24016

Ulrich, J.D., T.K. Ulland, T.E. Mahan, S. Nyström, K.P. Nilsson, W.M. Song, Y. Zhou, M. Reinartz, S. Choi, H. Jiang, et al. 2018. ApoE facilitates the microglial response to amyloid plaque pathology. *J. Exp. Med.* 215:1047–1058. https://doi.org/10.1084/jem.20171265

van den Brink, S.C., F. Sage, Á. Vértesy, B. Spanjaard, J. Peterson-Maduro, C.S. Baron, C. Robin, and A. van Oudenaarden. 2017. Single-cell sequencing reveals dissociation-induced gene expression in tissue subpopulations. *Nat. Methods.* 14:935–936. https://doi.org/10.1038/nmeth.4437

Vogl, T., K. Tenbrock, S. Ludwig, N. Leukert, C. Ehrhardt, M.A.D. van Zoelen, W. Nacken, D. Foell, T. van der Poll, C. Sorg, and J. Roth. 2007. Mrp8 and Mrp14 are endogenous activators of Toll-like receptor 4, promoting lethal, endotoxin-induced shock. *Nat. Med.* 13:1042–1049. https://doi.org/10.1038/nm1638

Zenaro, E., E. Pietronigro, V. Della Bianca, G. Piacentino, L. Marongiu, S. Budui, E. Turano, B. Rossi, S. Angiari, S. Dusi, et al. 2015. Neutrophils promote Alzheimer's disease-like pathology and cognitive decline via LFA-1 integrin. *Nat. Med.* 21:880–886. https://doi.org/10.1038/nm.3913